
Flow, Turbulence and Combustion **66:** 393–426, 2001.
© 2001 *Kluwer Academic Publishers. Printed in the Netherlands.*

Coherent Vortex Simulation (CVS), A Semi-Deterministic Turbulence Model Using Wavelets ⋆

MARIE FARGE[1] and KAI SCHNEIDER[2]
[1]*Laboratoire de Météorologie Dynamique, Ecole Normale Supérieure de Paris, 24 rue Lhomond, 75231 Paris Cedex 05, France;* [2] *Laboratoire de Modélisation et Simulation Numérique en Mécanique & Centre de Mathématiques et d'Informatique, Université de Provence, 39 rue Joliot-Curie, 13453 Marseille Cedex 13, France*

Received 24 May 2000; accepted in revised form 8 October 2001

Abstract. In the spirit of Ha Minh's semi-deterministic model, we propose a new method for computing fully-developed turbulent flows, called Coherent Vortex Simulation (CVS). It is based on the observation that turbulent flows contain both an organized part, the coherent vortices, and a random part, the incoherent background flow. The separation into coherent and incoherent contributions is done using the wavelet coefficients of the vorticity field and the Biot–Savart kernel to reconstruct the coherent and incoherent velocity fields. The evolution of the coherent part is computed using a wavelet basis, adapted at each time step to resolve the regions of strong gradients, while the incoherent part is discarded during the flow evolution, which models turbulent dissipation. The CVS method is similar to LES, but it uses nonlinear multiscale band-pass filters, which depend on the instantaneous flow realization, while LES uses linear low-pass filters, which do not adapt to the flow evolution. As example, we apply the CVS method to compute a time developing two-dimensional mixing layer and a wavelet forced two-dimensional homogeneous isotropic flow. We also demonstrate how walls or obstacles can be taken into account using penalization and compute a two-dimensional flow past an array of cylinders. Finally, we perform the same segmentation into coherent and incoherent components in a three-dimensional homogeneous isotropic turbulent flow. We show that the coherent components correspond to vortex tubes, which exhibit non-Gaussian statistics and long-range correlation, with the same $k^{-5/3}$ power-law energy spectrum as the total flow. In contrast, the incoherent components correspond to an homogeneous random background flow which does not contain organized structures and presents an energy equipartition together with a Gaussian PDF of velocity. This justifies their elimination during the CVS computation to model turbulent dissipation.

Key words: coherent structures, Coherent Vortex Simulation (CVS), semi-deterministic model, turbulence, wavelets.

1. Introduction

Computing fully-developed turbulent flows is one of the challenges for scientific computing. The difficulty comes from the nonlinear dynamics of the Navier–Stokes equations which excites a very large range of temporal and spatial scales. Turbu-

⋆ In memory of Ha Minh, with all our gratitude for the human and scientific treasures he has transmitted to us.

lence models are necessary because Direct Numerical Simulation (DNS) of fully-developed turbulent flows requires resolution which is out of the reach of present or next generation supercomputers. Turbulence models used in industrial codes are based on phenomenology, rather than first principles, and thus require tuning of their parameters for each flow configuration.

Laboratory and numerical experiments have shown that, whatever their space dimension, geometry or Reynolds number, turbulent flows exhibit self-organization, that leads to the formation of coherent structures, which play an essential role in the flow dynamics, and should be taken into account when modelling turbulence. One of the difficulties in dealing with coherent structures is that there are several definitions of them, based on statistical or dynamical points of view, or both. In the present paper we propose a definition of coherent structures based on a nonlinear filtering of the vorticity field projected into wavelet space. We call them 'coherent vortices' to avoid confusion with the other definitions.

Turbulent flow simulations can be divided into three classes:

- fully deterministic simulations, in which all scales of motion are resolved and deterministically computed, thus is DNS (Figure 1e);
- semi-deterministic methods, in which some degrees of freedom are deterministically computed while the influence of the others is modelled; among them are Large Eddy Simulation (LES, (Figure 1c) and Unsteady Reynolds Averaged Navier–Stokes equations (URANS, (Figure 1b); and
- fully statistical models, such as Reynolds Averaged Navier–Stokes equations (RANS (Figure 1a), in which only a steady solution of the mean turbulent flow fields is deterministically computed and the influence of all turbulent fluctuations is modelled.

These simulations are characterized by different computational costs, and a decreasing level of information on the turbulent motions, respectively. The most demanding method is DNS, for which the number of degrees of freedom to be computed at each time step is $N = c\,\mathrm{Re}$ for two-dimensional isotropic turbulent flows and $N = c\,\mathrm{Re}^{9/4}$ for three-dimensional isotropic turbulent flows, c being a constant which depends on the numerical scheme, and Re the Reynolds number of the flow. Therefore the maximal computable Reynolds number is limited by the CPU performance and memory of the computers. The number of degrees of freedom needed by LES does not depend on the Reynolds number, as long as one does not resolve the viscous boundary sublayers. Therefore LES allows one to compute much higher Reynolds number flows than DNS. The least demanding approach in terms of computational cost is RANS, as only the steady mean flow is computed. RANS does not take into account the spatial distribution of coherent vortices, while URANS and LES compute only a smoothed spatial distribution of them.

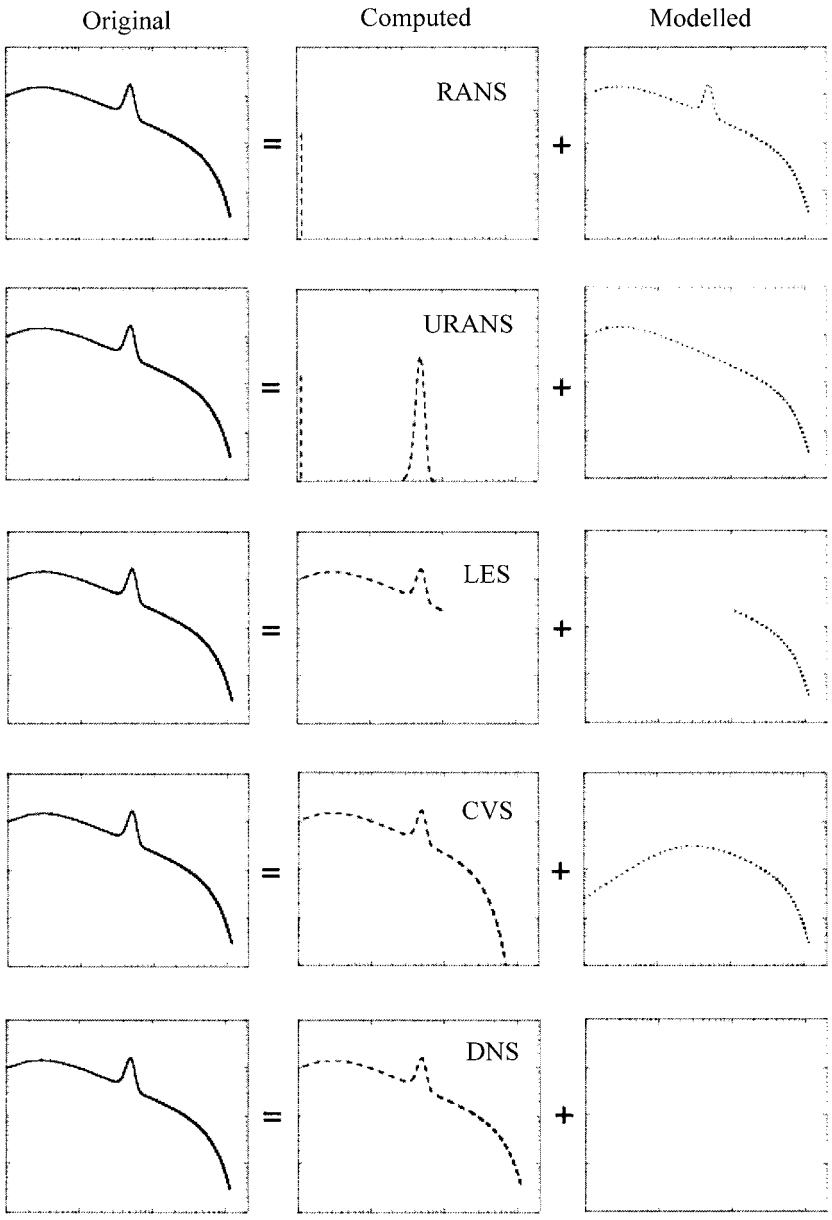

Figure 1. Comparison between several methods to compute turbulent flows: (a) RANS, (b) URANS, (c) LES, (d) CVS, (e) DNS.

We think that the semi-deterministic methods offer a good compromise, providing more physical insight than RANS and more realistic Reynolds numbers and computational cost than DNS. In this paper we argue that semi-deterministic methods can be improved by:

- better characterizing the coherent structures to be deterministically computed; and
- controlling the Gaussianity and the decorrelation of the discarded modes to be modelled.

As example we propose a new semi-deterministic method, called Coherent Vortex Simulation (CVS, (Figure 1d), aimed at this. It is based on a nonlinear wavelet filtering of the Navier–Stokes equations which extracts coherent vortices without imposing an *a priori* cut-off scale. The only *a priori* demand is to require a quasi-Gaussian probability distribution of the discarded incoherent components and decorrelation between them. The principle of CVS is:

- to deterministically compute the evolution of the coherent vortices in a wavelet basis, which dynamically adapts to the regions of strong gradients and thus resolves the nonlinear interactions between coherent vortices; and
- to model the influence of the incoherent components, produced by nonlinear vortex interactions, which are discarded at each time step.

The paper is organized as follows: after a short overview of classical turbulence models, we explain the CVS method and illustrate its applicability to both two- and three-dimensional turbulent flows. We present the CVS computation of a two-dimensional mixing layer and compare the results thus obtained with classical DNS. We also give a method of computing turbulent flows in complex geometries and use as an example the computation of a two-dimensional flow past an array of cylinders. Finally, we demonstrate the application of CVS to three-dimensional flows, and present the extraction of coherent vortex tubes in a three-dimensional homogeneous isotropic turbulent flow.

2. Classical Turbulence Models

2.1. PRINCIPLE

Even with present supercomputers, Navier–Stokes equations cannot be integrated in the fully-developed turbulence regime without using some *ad hoc* turbulence model. The role of turbulence model is to reduce the number of degrees of freedom of the system of equations to be computed. The degrees of freedom are split into two subsets: the retained modes, to be deterministically computed, and the discarded modes, whose effect is modelled. The number of retained modes should be as small as possible, while the number of discarded modes should be as large

as possible. Moreover, the discarded modes should have reached some statistical equilibrium state in order that their effect on the retained modes can be modelled. Therefore the central question is: which information should be kept, and which information can be safely discarded? A related question is: which averages or filterings are appropriate to compute the evolution of turbulent flows? We believe that these questions cannot be answered *a priori*. The answers must be based on a deep understanding of the nature of Navier–Stokes solutions at large Reynolds numbers, which results from a subtle interaction between the nonlinear term, the linear term and the incompressibility condition.

The statistical theory of homogeneous isotropic turbulence is based on ensemble averages, although in practice they are often replaced by space or time averages, which are equivalent, assuming ergodicity and Taylor's hypothesis. This theory relies on the cascade hypothesis, which supposes that an L^2-norm averaged quantity (energy in three dimensions or enstrophy in two dimensions) is injected at low wavenumbers and dissipated at high wavenumbers. This hypothetical spectral separation, between production at low wavenumbers and dissipation at high wavenumbers, allows the existence of an intermediate range of wavenumbers, called the inertial range, where the turbulent flow dynamics is supposed to be conservative and exhibits a power-law energy spectrum. This uni-directional cascade, from low wavenumbers to high wavenumbers, is observed in laboratory experiments using L^2-norm averages. However, if one considers the time evolution of one realization only, as is the case for numerical experiments, this direct cascade mechanism is no longer adequate. At each instant there is also backscatter [6, 34], which corresponds to transfers (of enstrophy in two dimensions or energy in three dimensions) in the opposite direction, i.e., from high to low wavenumbers. This backscatter comes from the nonlinear term of the Navier–Stokes equations, which instantaneously redistributes any quantity amongst all Fourier modes, because the nonlinear term in physical space becomes a convolution in spectral space which involves all Fourier modes. The cascade mechanism makes sense for ensemble averages, but it cannot be used to model the effect of the discarded modes on the retained modes, since those are instantaneous and correspond to one realization only.

In turbulence models (e.g., RANS, URANS or LES) one supposes that most of the modes can be discarded, provided that some term(s) or new equations(s) are added to model the effect of the discarded modes on the retained modes (Figure 1). In order to reduce the computational cost as much as possible, the number of retained modes should be much smaller than the number of discarded modes. Furthermore, the turbulence model will be efficient if the number of retained modes increases more slowly with the Reynolds number Re than does the total number of modes N. We have conjectured [28] that this is the case for two-dimensional turbulent flows filtered with wavelets, because the number of retained modes is roughly proportional to the number of vortices, which increases more slowly with Re than the total number of modes N. The retained modes are computed deterministically, while the effect of the discarded modes is statistically modelled. To justify this

procedure, it is assumed that the modelled modes are slaved to the resolved modes, and therefore are dynamically passive, in the sense that their nonlinear behaviour is very weak and should not significantly affect the resolved modes. Therefore one must insure that the discarded modes to be modelled have reached a statistical equilibrium state, characterized by a steady Gaussian Probability Distribution Function (PDF), and an equipartition of their energy (i.e., all degrees of freedom have the energy) which corresponds to decorrelation, similarly to a Gaussian white noise. In this case it is no longer necessary to compute the evolution of the discarded modes in detail, and the model describing the effect of the discarded modes on the retained modes can be specified once the mean and variance of the discarded modes have been parametrized in terms of the properties of the retained modes.

2.2. Reynolds averaged navier–stokes (rans)

The classical method for computing fully-developed turbulent flows is based on Reynolds averaging [37], which splits each flow field, e.g., velocity, into mean and fluctuations:

$$\mathbf{V} = \overline{\mathbf{V}} + \mathbf{V}', \tag{1}$$

where $\mathbf{V}$ is the mean and $\mathbf{V}'$ are the fluctuations.

To compute the mean, we consider

- either ensemble averages

$$\mathbf{V} = \int \mathbf{V}(\mathbf{x}, t)\, p(\mathbf{V})\, \mathrm{d}\mathbf{V}; \tag{2}$$

  where $p(\mathbf{V})$ is the PDF of $\mathbf{V}$;
- or time averages:

$$\mathbf{V} = \lim_{T\to\infty} \frac{1}{T} \int_0^T \mathbf{V}(\mathbf{x}, t)\, \mathrm{d}t; \tag{3}$$

- or space averages:

$$\mathbf{V} = \frac{1}{V_0(\Omega)} \int_\Omega \mathbf{V}(\mathbf{x}, t)\, \mathrm{d}\mathbf{x}, \tag{4}$$

  where $V_0(\Omega)$ denotes the volume of the computational domain Ω.

The goal is to calculate the mean velocity using a deterministic equation, and to design a statistical model, which simulates the effect of the fluctuations (which have been averaged out) on the mean. statistical turbulence model is necessary, because the huge number of degrees of freedom Reynolds number turbulent flows

prohibits to perform DNS. We briefly summarize the classical turbulence models and use a representation introduced by Ha Minh [27] to compare them (Figure 1).

If we compute only a steady mean solution, we have a RANS model (Figure 1a). If we compute the time evolution of the mean, we have a URANS model (Figure 1b). These models are extensively used for industrial applications, e.g., Reynolds stress or k–ϵ models. But it should be noticed that these low-order turbulence models lack universality, in the sense that the parameters of the model should be adjusted to fit laboratory measurements (e.g., in wind tunnel). This procedure must be repeated for each flow configuration, and sometimes different values of the parameters are required for different regions of the same flow [25].

Moreover, due to the nonlinearity of the Navier–Stokes equations, the fluctuations depend on the second-order moments, which depend on the third-order moments, and so on *ad infinitum*. Therefore the hierarchy of equations is not closed. Its closure requires that the statistics of the discarded moments be known completely. This is possible if their statistical distribution is Gaussian, since in this case all higher-order even moments can be expressed in terms of the second order moments and all odd moments are zero. Therefore the fundamental issue in turbulence modelling is to find an averaging technique that produces a fluctuating part with Gaussian statistics. Unfortunately, the classical averaging techniques do not guarantee this. In this paper we propose a nonlinear filtering method, based on the wavelet representation, which is designed to separate Gaussian from non-Gaussian fluctuations.

2.3. Semi-deterministic simulation (SDS)

The Semi-Deterministic Simulation (SDS) has been introduced by Ha Minh [26] following an idea proposed by Reynolds and Hussain [38], where each field is split into three contributions (Figure 1c):

$$\mathbf{V} = \mathbf{V} + \langle \mathbf{V} \rangle_C + \mathbf{V}', \tag{5}$$

with

- $\mathbf{V}$ being the time average;
- $\langle \mathbf{V} \rangle_C$ being a conditional average associated to the coherent structures; and
- $\mathbf{V}'$ corresponds to the remaining incoherent fluctuations.

SDS is appropriate for simulating turbulent flows when there exist dominant periodic modes, as it is the case for transitional flows close to the critical Reynolds number or periodically forced flows. Ha Minh [27] was considering phenomena having a characteristic temporal frequency, for instance to a periodic forcing, and he used the phase averaging procedure proposed by Reynolds and Hussain [38].

In this paper we propose a new semi-deterministic turbulence model with a conditional averaging method different from the one used by Ha Minh, although

the general principles of splitting between coherent and incoherent contributions is similar. The main difference is that our statistical approach is Bayesian [4] and the coherent vortices are extracted in each flow realization, using a procedure based on an *a priori* definition of coherent vortices in wavelet coefficient space. The classical approach is frequentist [4] and requires a sufficiently large statistical sample since the averaging is done *a posteriori*.

2.4. LARGE EDDY SIMULATION (LES)

Another approach to computing fully-developed turbulent flows is Large Eddy Simulation (LES) [19, 31], where the separation is done by means of linear filtering between large scale modes, assumed to be dynamically important, and small scale modes, assumed to be dynamically less important (Figure 1d). One should notice that the equivalence between large scale modes and low wavenumber modes is well defined for an ensemble of flow realizations, but is no more obvious for one flow realization. Since in numerical experiments we compute one flow realization at a time, we should be cautious when associating a large scale with a low wavenumber, which is valid for waves but not for individual vortices. Indeed, the vortices being localized in contrast to waves, one needs several wavenumbers to preserve their locality.

In LES the flow evolution is calculated deterministically up to a given cutoff scale λ, whereas the influence of the subgrid scales
($< \lambda$) on the resolved scales ($> \lambda$) is modelled, e.g., using Smagorinsky's parametrization. Each field (we consider velocity as example) is decomposed into

$$\mathbf{V}(\mathbf{x}, t) = \mathbf{V}_L(\mathbf{x}, t) + \mathbf{V}_H(\mathbf{x}, t), \tag{6}$$

where the low–pass filtered velocity is

$$\mathbf{V}_L(\mathbf{x}, t) = \int \mathbf{V}(\mathbf{x}', t) G_{>\lambda}(\mathbf{x}, \mathbf{x}')\, \mathrm{d}\mathbf{x}', \tag{7}$$

with $G_{>\lambda}$ a low–pass filter (e.g., Gaussian or box-filter) having a cutoff scale λ, and the high-pass filtered velocity is:

$$\mathbf{V}_H(\mathbf{x}, t) = \mathbf{V}(\mathbf{x}, t) - \mathbf{V}_L(\mathbf{x}, t). \tag{8}$$

This separation of the velocity into large and small scale contributions is not necessarily L^2-orthogonal, i.e., $(\mathbf{V}_L)_H \neq 0$ when filtering twice, and a nonzero interaction term $\langle \mathbf{V}_L, \mathbf{V}_H \rangle$ exists, as for example for the Gaussian filter. In this case the LES filter is no more idempotent, i.e., $(\mathbf{V}_L)_L \neq \mathbf{V}_L$ (as for example the Gaussian filter).

A drawback of LES filters is that they smooth strong gradients produced by nonlinear interactions and instabilities which may develop at subgrid scales are ignored. Indeed, LES models have problems dealing with backscatter, i.e., transfers from subgrid scales towards resolved scales owing nonlinear instabilities. The

dynamical LES model proposed by Germano et al. [22] takes backscatter into account, but only in a locally averaged way. In the next paragraph we propose a new method, called Coherent Vortex Simulation (CVS), adaptive in both space and scale, which overcomes this backscatter problem by insuring that aliasing errors remain negligible and that the discarded modes are decorrelated and in quasi-Gaussian statistical equilibrium.

3. Coherent Vortex Simulation (CVS)

3.1. Coherent vortex extraction

Inspired by the work of Grossmann and Morlet [24], we have proposed the use of wavelets to study turbulent flows [9, 11]. Wavelets are functions which are well localized in both physical and spectral space. In addition, their smoothness (defined by the number of times they can be differentiated without ultraviolet divergence) and their number of vanishing moments (defined by the number of times they can be integrated without infrared divergence) can be controlled. Lemarié and Meyer [32] has shown that one can construct orthogonal bases made from their translates and dilates. In this paper we will demonstrate that wavelet bases can efficiently represent data which are neither completely particle-like nor wave-like such as the coherent vortices observed in turbulent flows. Furthermore, fast wavelet algorithms in $O(N)$ exist and wavelet bases are available for Neumann or Dirichlet boundary conditions [5]. The advantage of the wavelet representation in comparison to the Fourier representation is that the phase information is built-in each wavelet coefficients, while it is carried by the combination of all Fourier coefficients otherwise. Therefore the spatial localization is preserved when one truncates wavelet series, which is not the case for Fourier series. For an introduction to wavelets we refer the reader to [3], and for a more advanced presentation to [33]. For an overview of the application of wavelets to the study of turbulence, we refer the reader to [11, 14, 15, 40].

We have designed a nonlinear wavelet filter, called CVS filter, able to extract coherent vortices and high strain regions from turbulent flows, using either the continuous wavelet transform [13] or the orthogonal wavelet transform [12]. We have shown [9, 10] that coherent vortices are multiscale and that a Fourier low-pass filter, as used in LES, eliminates the small scales of the coherent vortices. In contrast, the CVS filter is able to extract these vortices, without any smoothing, and leaves a quasi-homogeneous background flow free of organized structures, whose effect is therefore easier to model.

The procedures we have proposed for extracting coherent vortices are based on the wavelet decomposition of the vorticity, using either the continuous wavelet transform [13] or the orthogonal wavelet transform [12, 16]. We have chosen to work with the vorticity field, rather than the velocity field. We consider that vorticity is the most appropriate quantity to track the nonlinear dynamics of incompressible turbulent flows, whatever the space dimension, because it is independent of the

chosen inertial reference frame (Galilean invariance) and has strong topological properties expressed in Helmholtz' and Kelvin's theorems. The CVS extraction scheme is based on the assumption that coherent vortices are responsible for the non-Gaussianity of the PDF of vorticity in 2D and of velocity in 3D. We define the coherent vortices to be the non-Gaussian part, which corresponds to the modes remaining after discarding those with a Gaussian PDF. This is the only *a priori* assumption we make, apart from the choice of the wavelet basis. Note that we do not assume any shape, scale or intensity of the vortices.

To extract coherent vortices in two-dimensional turbulent flows we take the vorticity field $\omega(x, y) = \nabla \times \mathbf{V}$ and develop it as an orthogonal wavelet series, from the largest scale $l_{\max} = 2^0$ to the smallest scale $l_{\min} = 2^{J-1}$, using a two-dimensional multi-resolution analysis (MRA) of $L^2(R^2)$, i.e., a set of nested subspaces $V_j \subset V_{j+1}$ for $j = 0, \ldots, J-1$, and their orthogonal complement subspaces $W_j = V_{j+1} - V_j$ which correspond to the wavelet representation [5, 11]:

$$\omega(x, y) = \bar{\omega}_{0,0,0}\, \phi_{0,0,0}(x, y) + \sum_{j=0}^{J-1} \sum_{i_x=0}^{2^j-1} \sum_{i_y=0}^{2^j-1} \sum_{\mu=1}^{3} \tilde{\omega}^{\mu}_{j,i_x,i_y} \psi^{\mu}_{j,i_x,i_y}(x, y), \tag{9}$$

with

$$\phi_{j,i_x,i_y}(x, y) = \phi_{j,i_x}(x)\, \phi_{j,i_y}(y),$$

and

$$\psi^{\mu}_{j,i_x,i_y}(x, y) = \begin{cases} \psi_{j,i_x}(x)\, \phi_{j,i_y}(y); & \mu = 1, \\ \phi_{j,i_x}(x)\, \psi_{j,i_y}(y); & \mu = 2, \\ \psi_{j,i_x}(x)\, \psi_{j,i_y}(y); & \mu = 3, \end{cases} \tag{10}$$

where $\phi_{j,i}$ and $\psi_{j,i}$ are the one-dimensional scaling functions and the corresponding wavelets, respectively, and μ indexes the three spatial directions (horizontal, vertical and diagonal). Due to the orthogonality, the scaling coefficients are given by $\bar{\omega}_{0,0,0} = \langle \omega, \phi_{0,0,0} \rangle$ and the wavelet coefficients are given by $\tilde{\omega}^{\mu}_{j,i_x,i_y} = \langle \omega, \psi^{\mu}_{j,i_x,i_y} \rangle$, where $\langle \cdot, \cdot \rangle$ denotes the L^2-inner product. The scaling coefficients $\bar{\omega}_0$ correspond to an approximation of $\omega(x, y)$ at the largest scale $j = 0$. The wavelet coefficients $\tilde{\omega}_j$ correspond to the details to be added to approximate $\omega(x, y)$ from scale j to smaller scale $j + 1$.

We then split the vorticity field into two orthogonal components:

$$\omega = \omega_C + \omega_I. \tag{11}$$

The coherent vorticity ω_C is reconstructed by inverse wavelet transform from the wavelet coefficients $\tilde{\omega}^{\mu}_{j,i_x,i_y}$ whose modulus is larger than the threshold $\epsilon_T = \epsilon_0 Z^{1/2}$ with $\epsilon_0 = (2 \log_e N)^{1/2}$, where $Z = 1/2 \langle \omega, \omega \rangle$ is the total enstrophy and N the number of degrees of freedom or grid points. The incoherent vorticity ω_I is reconstructed from the remaining weak wavelet coefficients. The choice of the

threshold ϵ_T is based on theorems derived by Donoho and Johnstone [7, 8] for denoising in presence of Gaussian white noise. The advantage of the CVS filter is that there is no parameter to adjust since the threshold ϵ_T is objective, depending only on the total enstrophy and resolution. The orthogonality between ω_C and ω_I ensures a separation of the total enstrophy into $Z = Z_C + Z_I$.

We finally reconstruct both the coherent and the incoherent velocity fields using Biot–Savart kernel:

$$\mathbf{V}_C = \nabla^{\perp}\nabla^{-2}\omega_C \tag{12}$$

and

$$\mathbf{V}_I = \nabla^{\perp}\nabla^{-2}\omega_I, \tag{13}$$

where $\nabla^{\perp} = (-\partial_y, \partial_x)$ and ∇^{-2} denotes the Green's function of the Laplacian. It follows that:

$$\mathbf{V} = \mathbf{V}_C + \mathbf{V}_I. \tag{14}$$

This decomposition of the velocity field is only approximately orthogonal, i.e., $E = E_C + E_I + \varepsilon$ with $E = 1/2\langle \mathbf{V}, \mathbf{V}\rangle$ with $\varepsilon/E \ll 1$. This is due to the fact that the Biot–Savart kernel projected on a wavelet basis is almost diagonal. Note that, for the Fourier projection, it is diagonal and hence $\varepsilon = 0$ in this case.

As example, we apply the CVS filter to DNS data of a two-dimensional homogeneous and isotropic turbulenct flow, which was computed using a pseudo-spectral scheme with resolution $N = 512^2$ and without hyperdissipation. One realization of the vorticity field is shown in Figure 2a (left) and most of the enstrophy is concentrated in the coherent vortices one observe. We observe that:

- The coherent vortices are extracted by retaining only 2% of the N wavelet modes, which contain 99.99% of the total energy and 99.01% of the total enstrophy (Figure 2a, middle). They have the same velocity and vorticity PDFs (Figure 2c), the same energy spectrum in the inertial range (Figure 2d, left) and the same cross PDF between vorticity and streamfunction characteristic of coherence (Figure 2b) as the total flow.
- The remaining incoherent background flow is made of vorticity filaments densely distributed in space (Figure 2d, right), deprived of coherence (Figure 2b, right), which have Gaussian PDFs for both velocity (Figure 2c, left) and vorticity (Figure 2c, right), and present a k^{+1} scaling of the energy spectrum characteristic of enstrophy equipartition in two dimensions (Figure 2d, left). This gives evidence that the incoherent background flow has reached a statistical equilibrium which corresponds to turbulent dissipation.

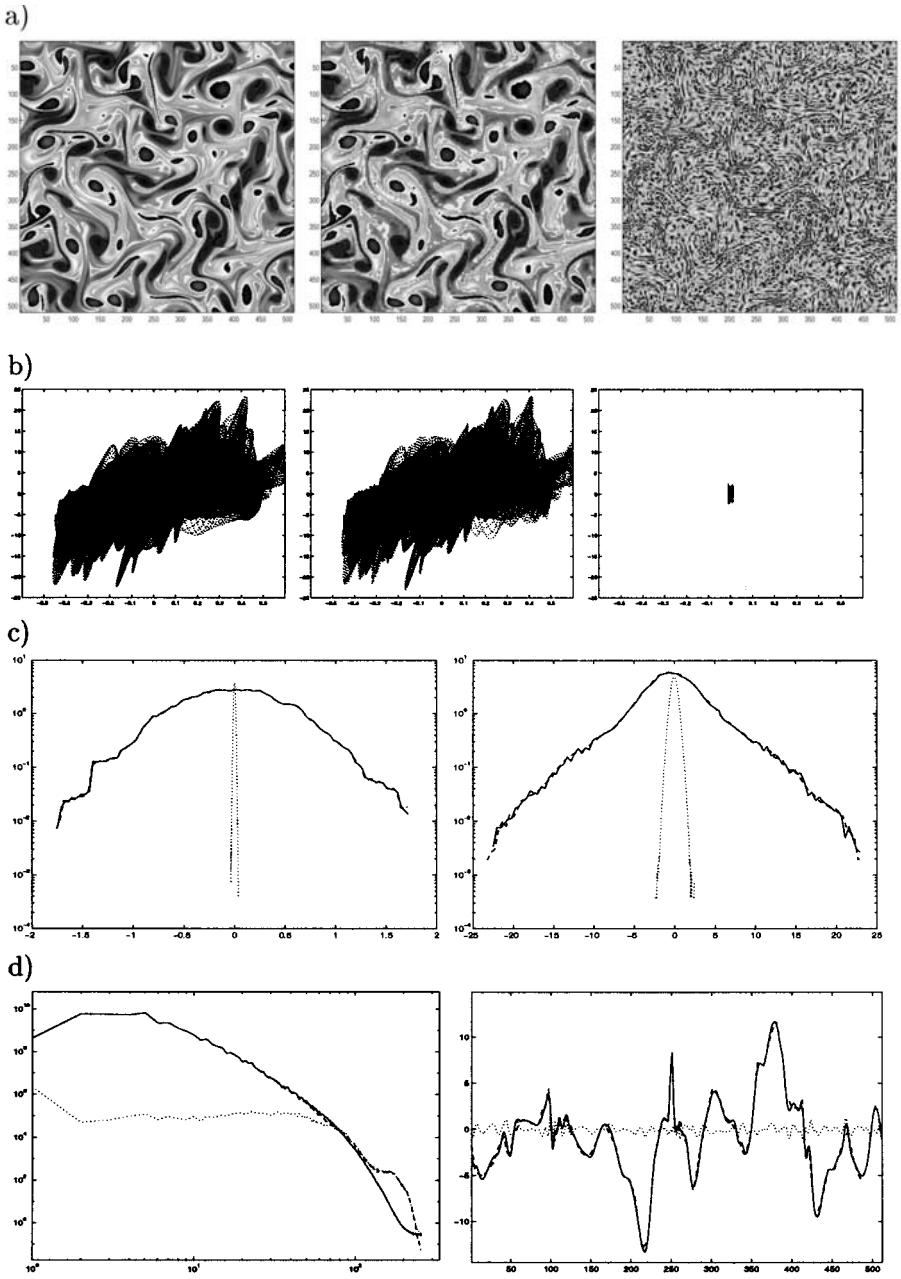

Figure 2. CVS filtering of a two-dimensional turbulent flow computed at $N = 512^2$: (a) total vorticity (left), coherent vorticity (middle) which corresponds to 2% N modes and contains 99% of both energy and enstrophy, incoherent vorticity (right) which corresponds to 98% N modes and contains less than 1% of both energy and enstrophy, (b) corresponding coherence scatter plots, (c) PDF of velocity (left), PDF of vorticity (right), (d) energy spectrum (left), cuts of vorticity (right). Solid lines for the total, dashed lines for the coherent and dotted lines for the incoherent contributions.

3.2. ADAPTIVE WAVELET COMPUTATION

The extraction of coherent vortices led us to propose a new way to split the turbulent flow dynamics into two parts:

- active coherent vortex modes, computed in a wavelet basis that is dynamically adapted at each time step (see Section 3.2),
- passive incoherent modes, which are discarded and whose effect on the coherent modes is modelled (see Section 3.4).

This approach, called Coherent Vortex Simulation (CVS) [16], differs significantly from LES. LES is based on low-pass filtering and assumes that the small scale dynamics can be represented in terms of the large scale dynamics (Figure 1c). But LES does not guarantee that the retained modes (larger than the cutoff scale λ) have a PDF similar to that of the total field and that the discarded modes (smaller than the cutoff scale λ) have a Gaussian PDF. CVS uses nonlinear filtering (defined in wavelet space) between Gaussian and non-Gaussian modes having different scaling laws, but without assuming *a priori* any spectral gap nor scale separation (Figure 1d). The goal of the CVS method compared to LES is to reduce the number of computed active modes for a given Reynolds number [12] and to guarantee the quasi-Gaussianity and the decorrelation of the incoherent degrees of freedom to be modelled [16].

For the numerical simulation of two-dimensional turbulence we consider the Navier–Stokes equations written in velocity-vorticity formulation:

$$\partial_t \omega + \nabla \cdot (\omega \mathbf{V}) - \nu \nabla^2 \omega = \nabla \times \mathbf{F}, \tag{15}$$

$$\nabla \cdot \mathbf{V} = 0, \tag{16}$$

with $\mathbf{V}$ the velocity field, $\omega = \nabla \times \mathbf{V}$ the vorticity, $\mathbf{F}$ an external force, and ν the kinematic viscosity. We assume periodic boundary conditions in both directions.

For the time discretization we use finite differences with a semi-implicit scheme, i.e., backwards-differencing for the viscous term and Adams–Bashforth extrapolation for the nonlinear term, both of second order. We obtain:

$$(\gamma I - \nu \nabla^2)\omega^{n+1} = \frac{4}{3}\gamma \omega^n - \frac{1}{3}\gamma \omega^{n-1} - \nabla \cdot (\omega^\star \mathbf{V}^\star) + \nabla \times \mathbf{F}, \tag{17}$$

where

$$\omega^\star = 2\,\omega^n - \omega^{n-1} \tag{18}$$

and

$$\mathbf{V}^\star = 2\,\mathbf{V}^n - \mathbf{V}^{n-1}, \tag{19}$$

with time step Δt, $\gamma = 3/(2\Delta t)$ and I representing the identity.

For spatial discretization we use a Petrov–Galerkin scheme. Therefore the vorticity is developed into a set of trial functions and the minimization of the weighted residual of (17) requires that the projection on a space of test functions vanishes. As space of trial functions we employ a two-dimensional multiresolution analysis (MRA) and develop ω^n at time step n into an orthonormal wavelet series 15). The test functions θ^{μ}_{j,i_x,i_y} are defined as solutions of the linear part of equation (17):

$$(\gamma I - \nu\nabla^2)\theta^{\mu}_{j,i_x,i_y} = \psi^{\mu}_{j,i_x,i_y}. \tag{20}$$

This avoids assembling the stiffness matrix and solving a linear equation at each time step. The functions θ, called vaguelettes, are explicitly calculated in Fourier space and have similar localization properties as wavelets do. Furthermore, using a proper rescaling, they constitute a Riesz basis [21]. The solution of (17) then reduces to a simple change of basis:

$$\begin{aligned}\tilde{\omega}^{\mu,n+1}_{j,i_x,i_y} &= \langle \omega^{n+1}, \psi^{\mu}_{j,i_x,i_y}\rangle \\ &= \left\langle \left(\frac{2}{3}\gamma\omega^n - \frac{1}{3}\gamma\omega^{n-1} - \nabla\cdot(\omega^\star\mathbf{V}^\star) + \nabla\times\mathbf{F}\right), \theta^{\mu}_{j,i_x,i_y}\right\rangle. \end{aligned}\tag{21}$$

An adaptive discretization is obtained by applying at each time step a nonlinear wavelet thresholding technique, retaining only wavelet coefficients $\tilde{\omega}^{\mu,n}_{j,i_x,i_y}$ with absolute value above a given threshold $\epsilon = \epsilon_0 Z^{1/2}$, where ϵ_0 is a constant. For the next time step the index coefficient set (which addresses each coefficient in wavelet space) is determined by adding neighbours to the retained wavelet coefficients, consequently only those coefficients $\tilde{\omega}$ in (21), belonging to this extrapolated index set, are computed using the adaptive vaguelette decomposition [21]. The nonlinear term $\nabla\cdot(\omega^\star\mathbf{V}^\star)$ is evaluated by partial collocation on a locally refined grid. The vorticity $\omega^\star$ is reconstructed in physical space on an adaptive grid (Figure 3a, right) from its wavelet coefficients $\tilde{\omega}^\star$ (Figure 3b, left) using the adaptive wavelet reconstruction algorithm [21]. From the adaptive vaguelette decomposition with $\theta = (\nabla^2)^{-1}\psi$, we solve $\nabla^2\Psi^\star = \omega^\star$ to get $\tilde{\Psi}^\star$ and reconstruct $\Psi^\star$ on a locally refined grid (Figure 3b, right). Using these special test functions θ avoids solving an elliptic problem as θ is calculated explicitly in Fourier space. By means of centered finite differences of fourth order we finally compute $\nabla\omega^\star$ and $\mathbf{V}^\star = (-\partial_y\Psi^\star, \partial_x\Psi^\star)$ on the adaptive grid and we evaluate the nonlinear term pointwise. Subsequently (21) can be solved using the adaptive vaguelette decomposition.

Although the numerical method is Eulerian, based on a Galerkin scheme, its adaptive character, in both space and scale, allows us to track the displacements and deformations of flow regions dominated by strong gradients, as Lagrangian methods do. Let us also mention that the total complexity of the algorithm is of order $O(N_{\mathrm{ad}})$, where N_{ad} denotes the number of wavelet coefficients retained in the adapted basis. As the present implementation has not yet been optimized, the computing time at the resolution used here ($N = 256^2$) is not as effective as a classical spectral method.

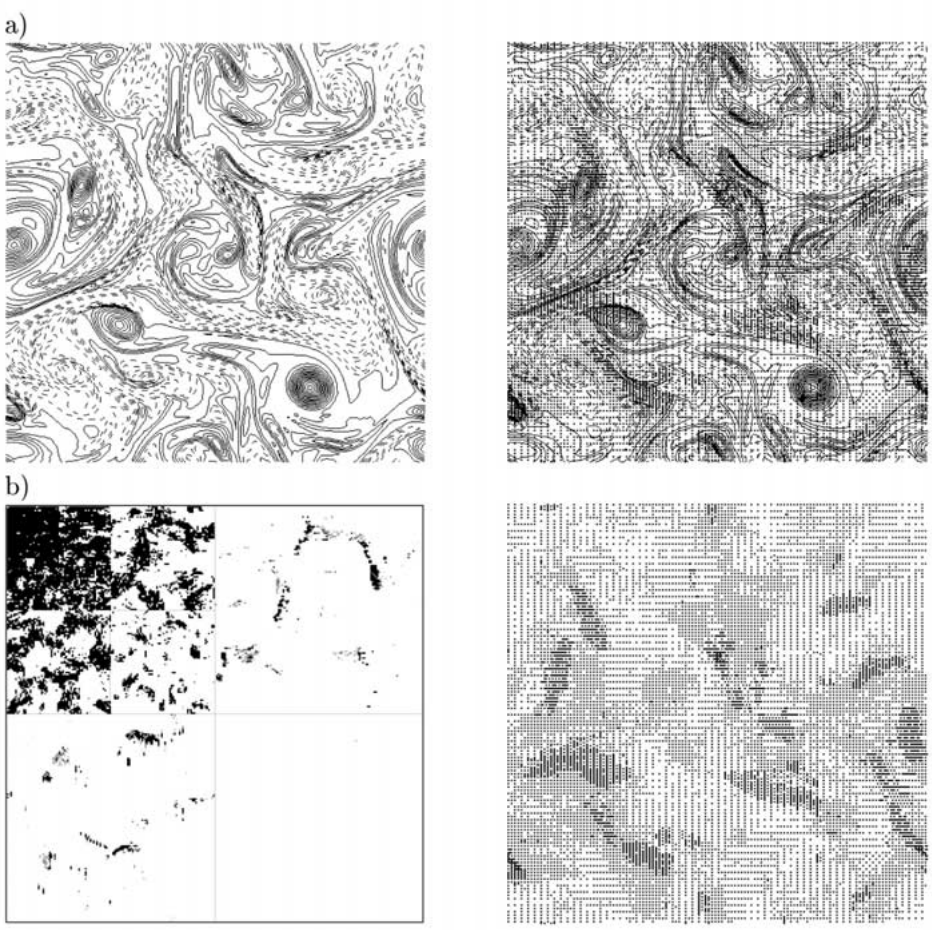

Figure 3. Decaying two-dimensional homogeneous and isotropic turbulence: (a) vorticity field (left) with the adaptive grid (right), (b) active wavelet coefficients (left) with the corresponding adaptive grid (right). The wavelet coefficients are represented using Mallat's convention [5, 33]: the smallest scales correspond to the largest squares (top-right for the vertical, bottom-left for the horizontal and bottom-right for the diagonal directions), while the largest scales correspond to the smallest squares (top-left).

To check the dynamical behaviour of the wavelet filtering we plot in Figure 4, besides the vorticity field ω, the linear dissipation $\nu\nabla^2\omega$ and the nonlinear advection term $\nabla \cdot (\omega \mathbf{V})$ of two-dimensional Navier–Stokes equations (15), together with the corresponding wavelet coefficients. We observe that the three wavelet coefficient fields exhibit a similar sparsity, i.e., the number of negligible wavelet coefficients increases when the scale decreases, which is a measure of intermittency [11, 41]. Moreover, we observe that the active structures in the small scales, which correspond to the strongest wavelet coefficients (Figure 4, right) have the same spatial support for the vorticity, for the linear dissipation and for the non-

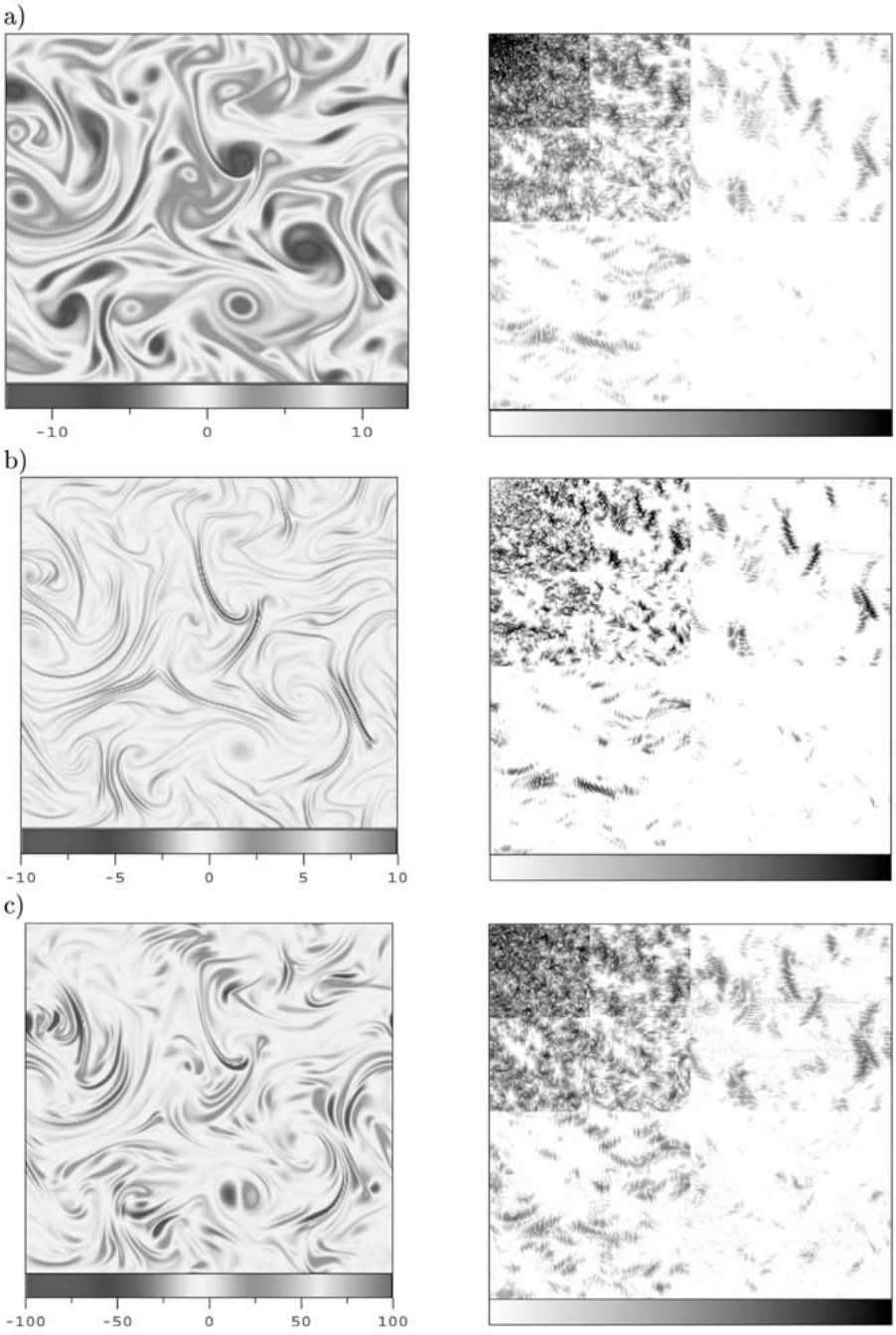

Figure 4. Wavelet analysis of two-dimensional homogeneous and isotropic turbulence: (a) vorticity, (b) linear dissipation term and (c) nonlinear advection term, with the corresponding wavelet coefficients on the right.

linear advection. This observation justifies to use a wavelet filter to compute their dynamics.

3.3. WAVELET FORCING

Forcing schemes are used to balance dissipation and reach statistically steady states. The usual method is performed in Fourier space by exciting Fourier modes in the two following ways:

- either a negative dissipation within a given wavenumber band, with a complex amplification coefficient which depends on the wavenumber; or
- a white or coloured noise in time with a prescribed isotropic spectral distribution and random phases, strongly peaked in the vicinity of a given wavenumber.

For both schemes the choice of the wavenumber band represents that part of the energy spectrum where the stiring has a significant effect. Neither of the two schemes is satisfactory because they both inject energy and enstrophy locally in Fourier space and therefore nonlocally in physical space. Another drawback is that the scale of the coherent vortices produced by the nonlinear dynamics is imposed by the scale at which the forcing is done. Our aim is to design a forcing scheme able to excite vortices locally in physical space and as smoothly as possible in order to avoid creating any unphysical discontinuities in the vorticity field. This is possible if the forcing is performed in wavelet space [42], rather than in Fourier space, as it is classically done.

To numerically simulate nondecaying two-dimensional turbulence we consider the Navier–Stokes equations (15) with an artificial dissipative term $\alpha\Psi$, called Rayleigh friction, to provide an energy sink at large scales, with the parameter α being the strength of the friction.

The forcing term $\nabla \times \mathbf{F}$ is applied at time step $n+1$ and is defined as a function of ω at time step n:

$$\nabla \times \mathbf{F}^{n+1}(\mathbf{x}) = \beta \sum_{J_0 < j < J_1} \sum_{k_x=0}^{2^j-1} \sum_{k_y=0}^{2^j-1} \sum_{\mu=1,2,3} \langle \omega^n, \psi^{\mu}_{j,k_x,k_y} \rangle \, \psi^{\mu}_{j,k_x,k_y}(\mathbf{x}), \tag{22}$$

with $0 \le J_0 \le J_1 \le J$, where J denotes the finest scale in the simulation, $\beta > 0$ and $|\langle \omega^n, \psi^{\mu}_{j,k_x,k_y} \rangle| > \epsilon$. The scale parameters J_0 and J_1 define the scale range of the forcing. The restriction to wavelet coefficients above a given threshold ϵ implies that only the dynamically active part of the flow, corresponding to the coherent vortices, is forced. The constants β and α, responsible for the strength of the forcing and the Rayleigh friction respectively, are adjusted in such a way that we obtain a statistically stationary state.

3.4. TURBULENCE MODEL

The CVS method is based on a deterministic computation of the evolution of the coherent flow components, while modelling the effect of the incoherent components on the coherent ones. In contrast to LES, CVS uses a nonlinear filter that depends on each flow realization, since it uses the wavelet thresholding procedure presented in Section 3.1. This CVS filter corresponds to an orthogonal projection, implying $(\omega_C)_I = 0$, and is hence idempotent, i.e., $(\omega_C)_C = \omega_C$, which is not the case for most LES filters (e.g., the Gaussian filter). It eliminates at each time step the incoherent components which are produced by the nonlinear interactions between the coherent components. This filtering thus models the turbulent dissipation, which corresponds to direct transfers (of enstrophy in 2D or energy in 3D) from the coherent to the incoherent components. Besides this, one should also model inverse transfers, from the incoherent to the coherent components, produced by the advection and straining of the random incoherent background by the coherent vortices which tend to reorganize it.

We apply the CVS filter to the two-dimensional Navier–Stokes equations, written in the vorticity-velocity formulation (15), and obtain the evolution equation for the coherent vorticity ω_C and coherent velocity $\mathbf{V}_C$:

$$\begin{aligned} &\partial_t \omega_C + \nabla \cdot (\omega\ \mathbf{V})_C - \nu \nabla^2 \omega_C = \nabla \times \mathbf{F}_C, \\ &\nabla \cdot \mathbf{V}_C = 0. \end{aligned} \tag{23}$$

For the nonlinear term $\nabla \cdot (\omega\ \mathbf{V})_C$ we use Leonard's triple decomposition, since it is computed with the same adapted grid as the linear term $\nu \nabla^2 \omega_C + \nabla \times \mathbf{F}_C$. Using (11) and (14) we decompose the nonlinear term of (23) into:

$$(\omega\ \mathbf{V})_C = \omega_C\ \mathbf{V}_C + L + C + R, \tag{24}$$

with the Leonard stress L, the cross stress C and the Reynolds stress R defined as:

$$\begin{aligned} L &= (\omega_C\ \mathbf{V}_C)_C - \omega_C\ \mathbf{V}_C, \\ C &= (\omega_I\ \mathbf{V}_C)_C + (\omega_C\ \mathbf{V}_I)_C, \\ R &= (\omega_I\ \mathbf{V}_I)_C. \end{aligned}$$

The sum of these unknown stresses corresponds to the incoherent stress to be modelled:

$$\tau_I = (\omega\ \mathbf{V})_C - \omega_C\ \mathbf{V}_C = L + C + R, \tag{25}$$

which describes the effect of the discarded incoherent components on the retained coherent components. Note that the localization property of the wavelet representation controls aliasing errors and therefore the Leonard stress L remains negligible since $(\omega_C\ \mathbf{V}_C)_C \simeq \omega_C\ \mathbf{V}_C$ [40].

The filtered Navier–Stokes equations (23) can be rewritten as:

$$\partial_t \omega_C + \nabla \cdot (\omega_C \, \mathbf{V}_C) - \nu \nabla^2 \omega_C = \nabla \times \mathbf{F}_C - \nabla \cdot \tau_I,$$
$$\nabla \cdot \mathbf{V}_C = 0. \tag{26}$$

We integrate equations (26) with the adaptive wavelet method described in Section 3.2, in retaining only the strong wavelet coefficients corresponding to the coherent components. The wavelet basis is remapped at each time step in order to follow, in both space and scale, the motion of the coherent vortices and to resolve the regions of strong gradients produced by their nonlinear interactions [39].

In contrast to LES, the incoherent stress τ does not correspond to turbulent dissipation, since CVS models it by eliminating the incoherent components at each time step. The incoherent stress τ here corresponds to a weak forcing, which models the reorganization of the random incoherent background due to its advection by the coherent vortices. We propose two different ways to model the incoherent stress τ:

- Solving an linear advection-diffusion equation for the incoherent vorticity ω_I by neglecting the influence of incoherent velocity terms to compute the interaction terms [40]. This approach is in the spirit of nonlinear Galerkin methods using a time scale splitting between the coherent and incoherent flow components. This is possible since the time evolution of the incoherent background, characterized by the time scale $t_I = (Z_I)^{-1/2}$, is much slower than the characteristic time scale $t_C = (Z_C)^{-1/2}$ of the coherent vortex motions, because $Z_C \gg Z_I$. This behaviour of the incoherent background flow had already been noticed, and discussed in comparison to Fourier filtering in [12, 40].
- Modelling the incoherent stress τ_I as a forcing term in wavelet space (see Section 3.3), proportional to the enstrophy discarded at the previous time step. This forcing term reinjects in an inhomogeneous way a small percentage of the incoherent enstrophy lost by the CVS filtering to model turbulent dissipation. This weak forcing models the reorganization of the incoherent background advected by the coherent vortices and thus contributes to the coherent energy.

The CVS method relies on the assumption that the incoherent part of the flow remains quasi-Gaussian. This is true for short times because the strain exerted by the coherent vortices on the incoherent background flow slows down the nonlinear interactions between incoherent modes [28]. This property has not yet been checked for three-dimensional turbulent flows, but we conjecture it is still valid in this case.

3.5. COMPLEX GEOMETRIES

Computing fully-developed turbulent flows in complex geometries is an important goal for CFD, since most industrial applications involve walls, obstacles or containers of different shapes. The problem of treating such flows with no-slip boundary conditions is still open, since Prandtl's classical wall law does not hold as soon as the boundary layer detaches, which is the case when the Reynolds number becomes large. Anyway, even when the boundary layer remains attached, its thickness is inversely proportional to the Reynolds number, which thus requires a prohibitive grid refinement near the wall.

To overcome these difficulties and to compute flows near walls or obstacles, we have proposed to combine the CVS method with a recently developed penalization method which offers an elegant way to take account of complex geometries. The penalization method was introduced in 1984 by Arquis and Caltagirone [2], who modelled solid walls or obstacles as a porous medium with porosity η tending to zero. It has been implemented using finite differences [2], finite volumes [1] and spectral methods [20, 29, 45]. This volume penalization is different from the surface penalization introduced by Peskin [36] and from the immersed boundary methods, using Lagrange multipliers, proposed by Glowinski [23]. The complex geometry is described by a mask function $\chi(\mathbf{x})$ set to 1 inside the solid regions and to 0 elsewhere, which can also take into account obstacles whose shape varies in time, such as flaps or actuators, by varying the mask when time evolves.

We thus solve the Navier–Stokes equations with an additional penalization term

$$\partial_t \mathbf{V}_\eta + (\mathbf{V}_\eta \cdot \nabla)\mathbf{V}_\eta + \nabla P_\eta - \nu \nabla^2 \mathbf{V}_\eta + \frac{1}{\eta}\chi(\mathbf{x})\mathbf{V}_\eta = \mathbf{F}. \tag{27}$$

For $\eta \to 0$ the flow evolution is governed by Navier–Stokes equations in regions where the fluid is, and by d'Arcy law (velocity proportional to pressure gradient) in regions where the obstacles or solid walls are.

The penalization term thus forces the velocity to be very small inside solid regions, which leads to the formation of boundary layers where the flow encounters the solid walls. Recently Angot et al. [1] have demonstrated that, when $\eta \to 0$, the solutions of the penalized Navier–Stokes equations tend to the solutions of the Navier–Stokes equations with no-slip conditions on obstacles or solid walls.

Modelling turbulent flows in the vicinity of walls is crucial for predicting and controlling their evolution, e.g., to compute the drag and lift induced by obstacles or to compute heat exchanges in unsteady regime.

The resulting forces $\mathbf{R}$ on the obstacle can be computed by integrating the penalized velocity over the obstacle's volume [1]:

$$\mathbf{R} = \lim_{\eta \to 0} \int_{\Omega_s} \nabla P_\eta \, \mathrm{d}\mathbf{x} = -\lim_{\eta \to 0} \frac{1}{\eta} \int_{\Omega_s} \mathbf{V}_\eta \, \mathrm{d}\mathbf{x} = \int_{\partial\Omega_s} S(\mathbf{V}, P) \cdot \mathbf{n} \, \mathrm{d}\gamma, \tag{28}$$

where Ω_s denotes the volume of the obstacle, $\partial\Omega$ its boundary, $\mathbf{n}$ its outer normal and

$$S(\mathbf{V}, P) = \frac{1}{2\nu}\left(\nabla\mathbf{V} + (\nabla\mathbf{V})^T\right) - PI$$

the stress tensor. Therefore the drag and the lift induced by the obstacle are easy to compute as volume integrals instead of contour integrals.

For the application of the penalization method to two-dimensional turbulent flows we prefer to use the vorticity-velocity formulation [29], rather than the velocity-pressure formulation. Taking the curl of (27), we obtain

$$\partial_t\omega_\eta + \mathbf{V}_\eta \cdot \nabla\omega_\eta - \nu\,\nabla^2\,\omega_\eta + \nabla \times \left(\frac{1}{\eta}\,\chi_{\Omega_s}\,\mathbf{V}_\eta\right) = \nabla \times \mathbf{F}. \tag{29}$$

Using the vector identity $\nabla \times (\zeta\,\nabla^\perp\phi) = \nabla \cdot (\zeta\nabla\phi)$ we get

$$\partial_t\omega_\eta + \mathbf{V}_\eta \cdot \nabla\omega_\eta - \nu\,\nabla^2\,\omega_\eta + \frac{1}{\eta}\nabla \cdot (\chi_{\Omega_s}\,\nabla\Psi) = \nabla \times \mathbf{F}, \tag{30}$$

where $\nabla^2\Psi = \omega$ and $\nabla^\perp\Psi = (-\partial_y\Psi, \partial_x\Psi) = \mathbf{V}$).

4. Applications of CVS

4.1. 2D TEMPORALLY DEVELOPING MIXING LAYER

We consider a temporally developing mixing layer, which is a flow configuration which has been well studied, and is therefore a good test case for the CVS method. The initial velocity $\mathbf{V} = u, v$ corresponds to a hyperbolic-tangent profile $u(y) = U\tanh(2y/\delta_0)$ which implies a vorticity thickness $\delta_0 = 2U/(\mathrm{d}u/\mathrm{d}y)|_{y=0}$. From linear stability analysis the mixing layer is known to be inviscidly unstable and any perturbation leads to the formation of vortices by Kelvin–Helmholtz instability, with the most amplified mode corresponding to a longitudinal wavelength $L = 7\delta_0$. To trigger the instability we have superimposed a weak white noise in the rotational region.

We compare three different simulations, i.e., a DNS as reference run and two CVS integrations, with and without turbulence model, which have been computed during 60 s, i.e., 30 eddy-turnover times based on the initial enstrophy. As turbulence model we use a forcing term in wavelet space previously described in Section 3.3. In all simulations the maximal resolution is $N = 256^2$, which corresponds to $J = 8$ octaves. For the wavelet projection we have chosen cubic spline wavelets of Battle–Lemarié [5, 33] and the threshold $\epsilon_T = \epsilon_0 Z^{1/2}$ for the wavelet coefficients has been set to the value $\epsilon_0 = 10^{-5}$. The viscosity is $\nu = 5{\cdot}10^{-5}\,\mathrm{m^2 s^{-1}}$, which allows a time step $\Delta t = 10^{-3}$ s. The initial vorticity thickness δ_0 is chosen such that ten vortices should develop in the periodic domain of size $[0, 2\pi]^2$.

In Figure 6c we compare the energy spectra at $t = 60$ s for the reference run, computed using a classical pseudo-spectral method, and for two CVS runs,

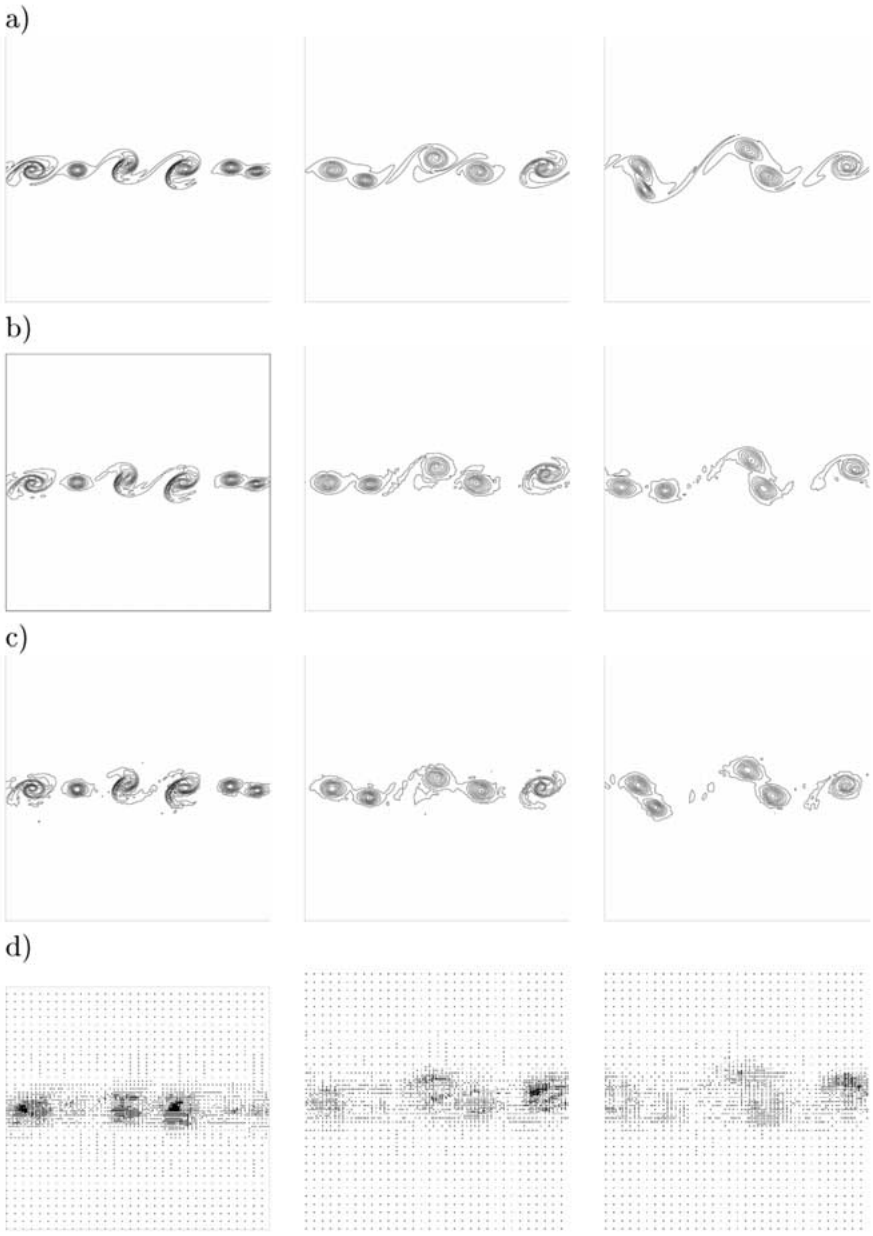

Figure 5. Simulation of a two-dimensional mixing layer: isolines of vorticity at $t = 30$ s (left), 50 s (middle) and 60 s (right) for (a) DNS, (b) CVS without turbulence model, (c) CVS with turbulence model, (d) corresponding adaptive grid.

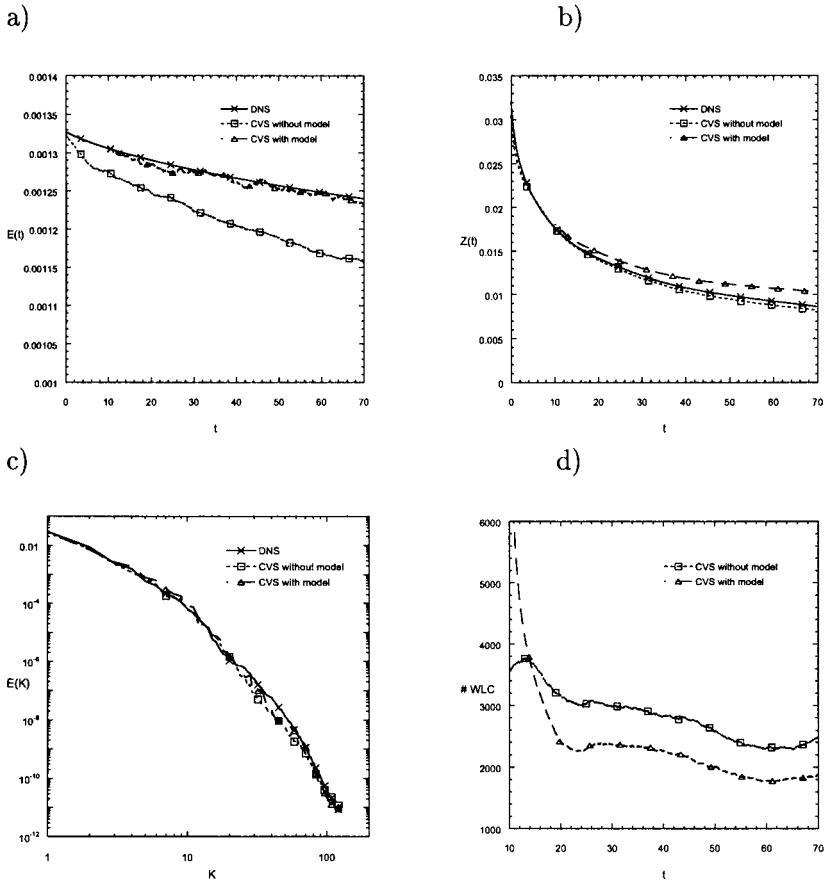

Figure 6. Comparison between DNS and CVS with and without turbulence model for the two-dimensional mixing layer: (a) time evolution of energy, (b) time evolution of enstrophy, (c) energy spectra at $t = 60$ s, (d) time evolution of the number of degrees of freedom for the two CVS computations.

computed with and without turbulence model. They show that all scales of the flow are well-resolved for both CVS runs but that the energy is underestimated in the absence of turbulence model. The underlying grid, which corresponds to the centers of the retained wavelets for the CVS runs, shows local refinement in regions of strong vorticity gradients, where dissipation is most active (Figure 5d). In Figure 5 we compare the evolutions of the vorticity field for the reference DNS (a), and for the CVS with (c) and without (b) the turbulence model. In all simulations, as predicted by the linear theory, ten vortices are formed at $t = 12$ s (not shown here), which subsequently undergo mergings. We observe that in the CVS run without the turbulence model the evolution of coherent vortices is slightly delayed with respect to the reference run. This is due to the fact that the retained wavelet coefficients contain less energy and enstrophy than the total flow, as observed in Figure 6 which

compare the time evolutions of the total energy (a) and enstrophy (b) in the three simulations. We observe that, if we do not model the effect of the discarded modes on the retained ones, there is a strong loss of energy (Figure 6b). For the CVS run with model the situation is somehow different. The flow evolution follows the reference and captures all of the vortex mergings (Figure 5c). This is also reflected in the time evolution of the energy and enstrophy. The wavelet forcing term injects enstrophy into the retained wavelet coefficients and leads to a slight increased of the enstrophy with respect to the reference run (Figure 6b). For the energy evolution we find a good agreement between the DNS and the CVS with turbulence model (Figure 6a).

For both CVS simulations (with and without turbulence model) we observe that the basis dynamically adapts to the flow evolution, although only 4% of the coefficients are used. In Figure 6d we plot the time evolution of the number of degrees of freedom for the two CVS runs. We observe an initial phase, up to $t = 12$ s in which there is a strong reduction in the number of retained modes, which corresponds to the formation of the coherent vortices and associated high strain regions. Later in time, the number of retained modes remains almost constant and represents a significant reduction in the number of modes, with $N_{\mathrm{ad}} = 2000$, out of $N = 65536$ initial modes, which corresponds to 3% of retained modes.

4.2. 2D HOMOGENEOUS ISOTROPIC TURBULENT FLOW

As an illustration of the CVS forcing we consider a two-dimensional homogeneous isotropic flow which is forced in wavelet space to obtain a statistically steady state. The resolution is $N = 256^2$ corresponding to $J = 7$, the viscosity $\nu = 2 \cdot 10^{-3}$ m^2 s^{-1} and $\Delta t = 10^{-3}$ s. The forcing scale range lies between $J_0 = 3$ and $J_1 = 6$ with $\beta = 2.5 \cdot 10^{-1}$ s^{-2} and $\alpha = 1.0$ m^{-2} s^{-1}. The wavelet decomposition is done using cubic spline wavelets of Battle–Lemarié type. The wavelet compression is done by cancelling all wavelet coefficients smaller than the threshold $\epsilon_0 = 10^{-4}$ s^{-1}.

Figure 7e shows that both energy and enstrophy are steady during more than 60 eddy turnover times. Figure 7a displays the vorticity field in the stationary regime at $t = 0$, 8 and 16 s, during which neither the energy spectrum (Figure 7c) nor the PDF of vorticity (Figure 7d) change significantly in time. The vortices present in the initial condition become more circular and isolated during the flow evolution, because they are better able to stand mutual strain due to the additional enstrophy injected into them. We observe that the slopes of the spectra (see Figure 7c) are much steeper (close to k^{-6}) than the k^{-3} law predicted by the statistical theory of homogeneous turbulence. This discrepancy confirms the fact that the spectral behaviour of two-dimensional turbulent flows is not universal and depends on the forcing.

We also observe that there is no inverse energy cascade, because the maximum of energy remains localized around wavenumber $k_I = 4$. This is different from

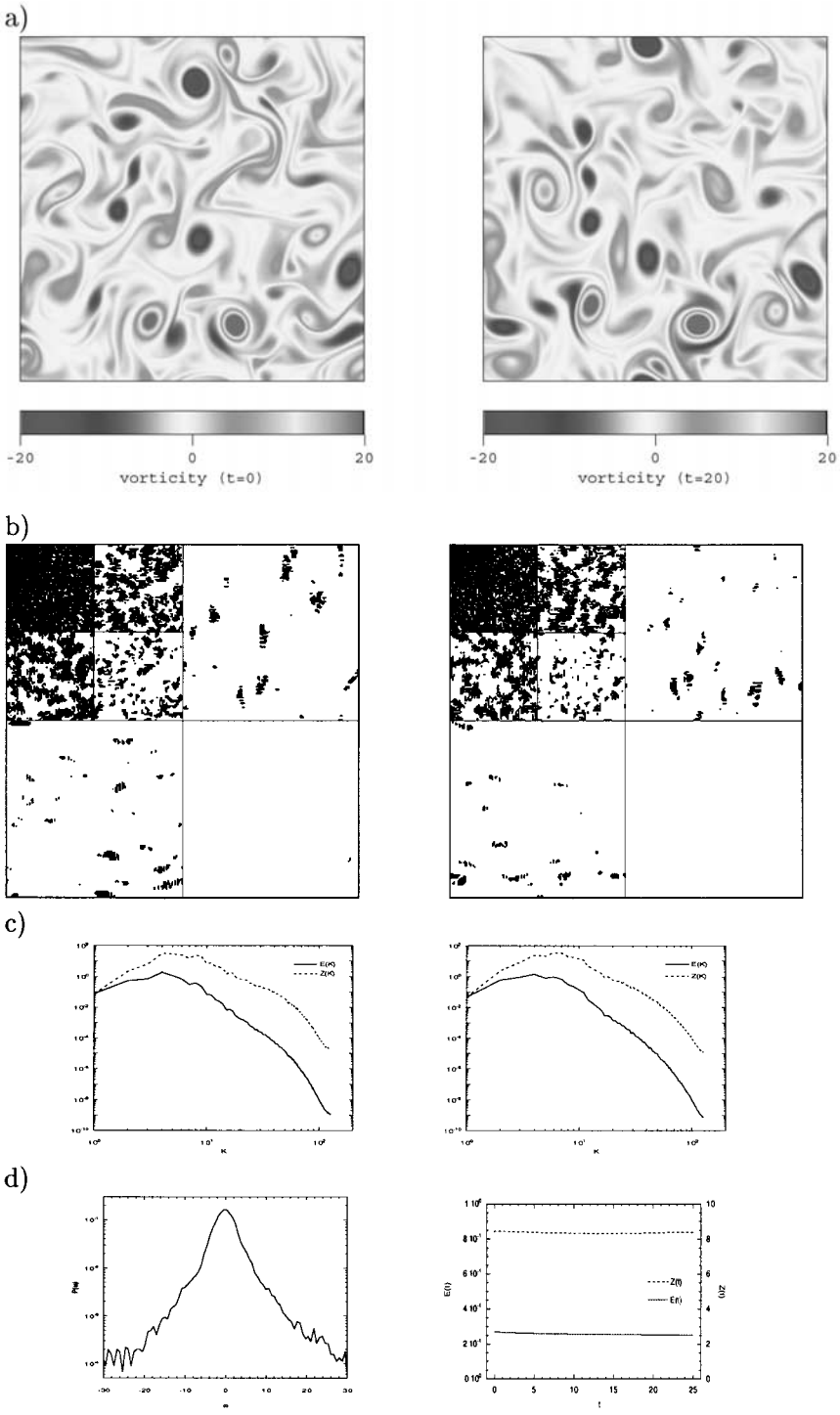

Figure 7. Wavelet-forced two-dimensional homogeneous and isotropic turbulence: (a) vorticity at $t = 0$ (left) and at $t = 20$ (right), (b) corresponding active wavelet coefficients, (c) corresponding energy and enstrophy spectra, (d) PDF of vorticity, (e) evolution of energy and enstrophy.

what is predicted by the statistical theory of homogeneous turbulence [30]. In Figure 7b we observe that the spatial support of the active wavelet coefficients decreases with the scale, which reveals a strong intermittency of the flow. Consequently the vorticity field is efficiently compressed in a wavelet basis, because only about 20% of the $N = 256^2$ coefficients are needed to represent the flow dynamics. We also show that the PDF of vorticity (Figure 7d) is Gaussian for the weak values, corresponding to the background flow, and presents non-Gaussian tails for the strong values, corresponding to the vortices.

4.3. 2D FLOW PAST AN ARRAY OF CYLINDERS

As example for the application of penalization to study complex geometries, we present several numerical simulations [45, 46] of a two-dimensional flow through an array of cylinders at $\mathrm{Re} = 1000$ (the Reynolds number being based on the diameter of the cylinders) for different angles of incidence, 0, 30, 45°. Note that for this flow configuration, which is typical for heat exchangers, the two-dimensional approximation is justified for Reynolds numbers up to several thousands. Figure 8a shows the corresponding instantaneous vorticity fields. We observe that the behaviour of the flow varies significantly depending on the angle of incidence. In particular, the time evolution of the drag (Figure 8b) and the lift coefficients (Figure 8c) are very different.

The advantage of the CVS method is to refine dynamically the grid in regions of strong gradients, even where the boundary layer detaches. The active wavelet coefficients (Figure 8d) and the corresponding grid in physical space (Figure 8e) illustrate the local refinment property in regions of strong gradients. This feature allows a better prediction of the vorticity production in wall regions, together with the boundary layer detachment, which are both essential for computing drag and lift coefficients.

4.4. 3D HOMOGENEOUS ISOTROPIC TURBULENT FLOW

The importance and the role of coherent structures (i.e., vortex tubes) in three-dimensional turbulence have been established largely by high resolution numerical simulations, e.g., in [47]. We consider DNS data of a statistically steady three-dimensional homogenous and isotropic turbulent flow. One realization of the vorticity field is shown on Figure 9a and most of the enstrophy is concentrated in the coherent vortex tubes. The flow was computed by Vincent and Meneguzzi [47] using a pseudo-spectral scheme with resolution $N = 256^3$ corresponding to a Taylor microscale Reynolds number $R = 150$. A 64^3 subcube from one realization of the vorticity field is shown in Figure 9a, where we observe that most of the enstrophy is concentrated in coherent vortex tubes.

We project each component of the vorticity field $\boldsymbol{\omega}$ on a three-dimensional orthogonal wavelet basis using Coifman 12 wavelets [5, 33], which are compactly

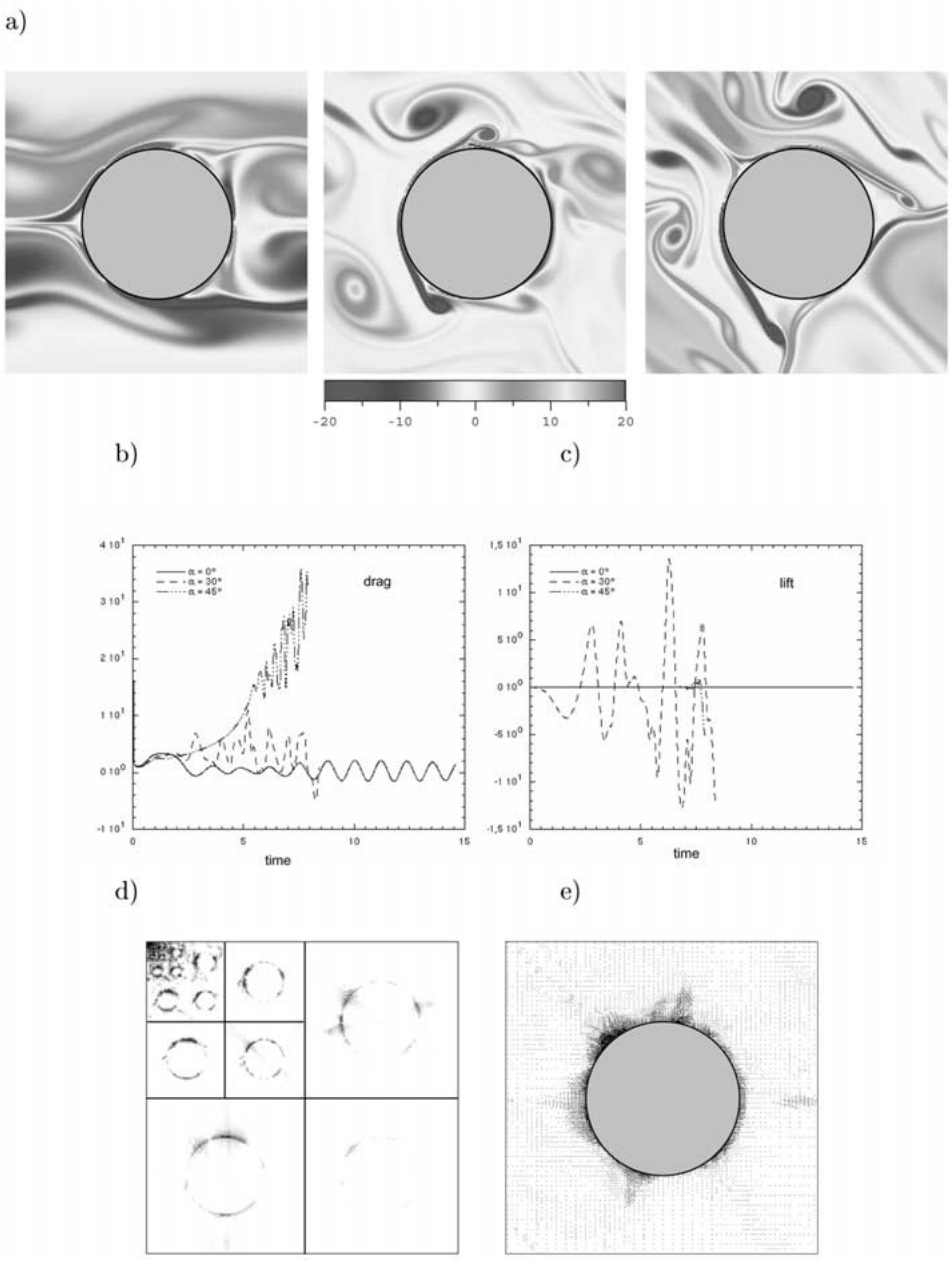

Figure 8. Computation of the flow past an array of cylinders for three angles of incidence α: (a) vorticity for $\alpha = 0°$ (left), 30° (middle), 45° (right), (b) drag, (c) lift, (d) wavelet coefficients of vorticity for $\alpha = 30°$, (e) adaptive grid for $\alpha = 30°$.

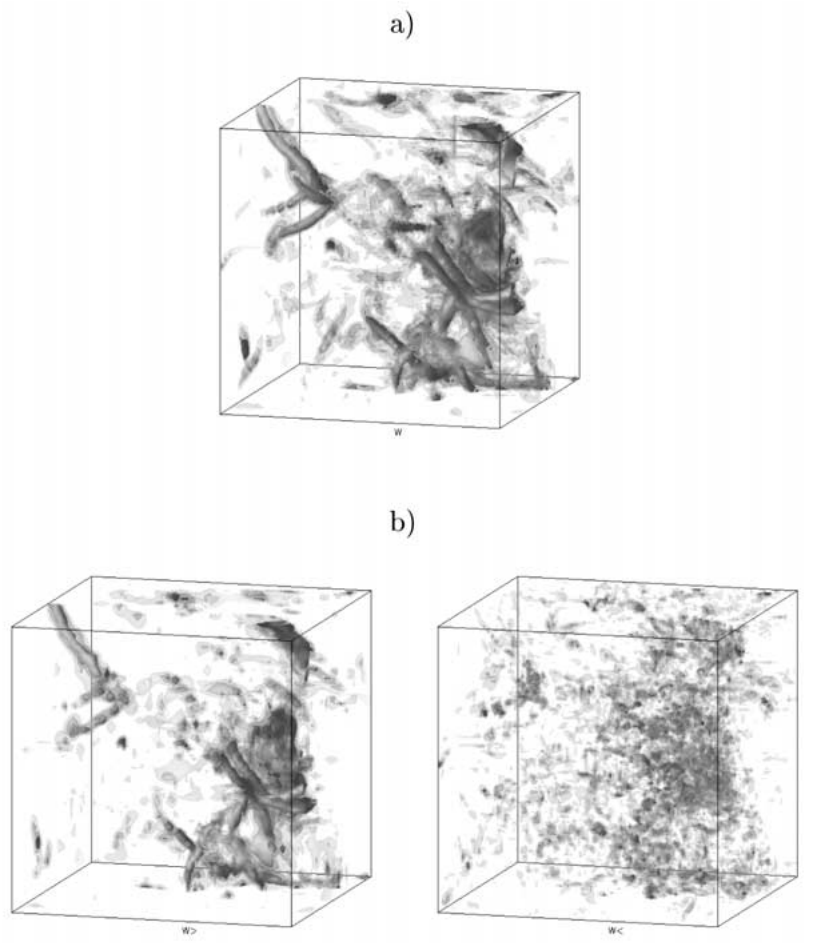

Figure 9. Homogeneous and isotropic three-dimensional turbulence: isosurfaces of vorticity modulus for (a) the total flow with $|\omega| = 2\sigma$ and $\sigma = (2Z)^{1/2}$, (b) the coherent flow with $|\omega| = 2\sigma$ (left) and incoherent flow with $|\omega| = \sigma$ (right).

supported, quasi-symmetric and have good spectral localization. We then reconstruct the coherent vorticity field ($\boldsymbol{\omega}_C$) from those wavelet coefficients for which the modulus of the wavelet coefficients is larger than $\epsilon_T = \epsilon_0 Z^{1/2}$ with $\epsilon_0 = (4/3 \log_e N)^{1/2}$, while the incoherent background flow ($\boldsymbol{\omega}_I$) is reconstructed from the remaining weak coefficients.

We find that only 3% of the coefficients extract the coherent vortex tubes (Figure 9b) which retain 99% of the energy and 75% of the enstrophy. The remaining 97% of the coefficients represent the incoherent background flow (Figure 9c) which is depleted from organized structures and contains only 1% of the energy and 25% of the enstrophy. We observe that both coherent and incoherent vorticity fields are weakly divergent, although the divergent part of the enstrophy is less than 3%

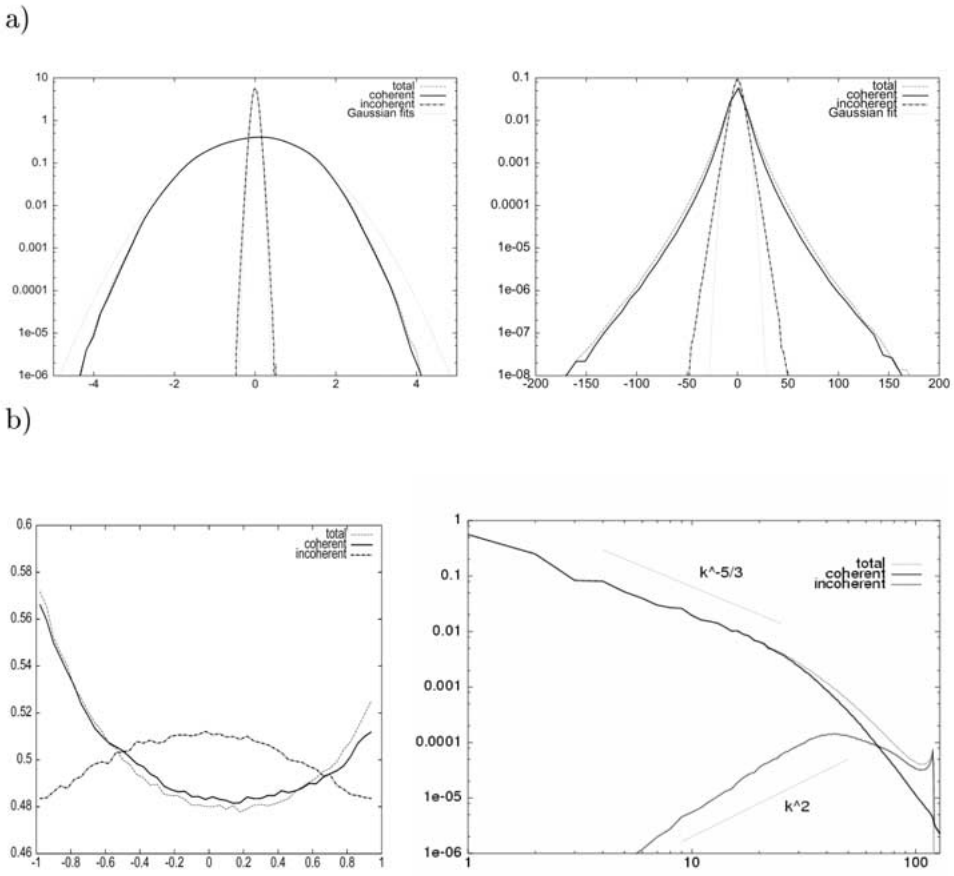

Figure 10. Superposition of the total, coherent and incoherent contributions to: (a) the PDF of velocity (left) and PDF of vorticity (right), (b) the PDF of relative helicity (left) and energy spectrum (right).

of the total enstrophy and affects only the dissipative scales. The same problem is encountered with vortex methods applied to three-dimensional turbulent flows [48]. However, the coherent and incoherent velocities remain divergence-free since they are reconstructed using the Biot–Savart's kernel.

The energy spectrum (cf. Figure 10b, right) shows that both coherent and incoherent components are multiscale, as previously observed for 2D turbulence [12]:

- the coherent flow exhibits the same power-law spectrum in $k^{-5/3}$ as the total flow;
- the incoherent flow has a k^{+2} power-law spectrum which corresponds to an equipartition of the incoherent energy in three dimensions.

The PDFs of velocity (Figure 10a, left) and of vorticity (Figure 10a, right) for the coherent part are the same as the original PDFs, which confirms that the statistical information is preserved by the CVS filter. In contrast, the PDF of the incoherent energy is Gaussian with a variance ten times smaller that for the total flow while the PDF of the incoherent vorticity is exponential with a variance also strongly reduced.

The CVS filter is based on a denoising method applied to the vorticity field without any *a priori* assumption as to the shape, topological or dynamical properties of the coherent structures to be filtered. We now use the relative helicity

$$h = \frac{\mathbf{V} \cdot \boldsymbol{\omega}}{|\mathbf{V}|\,|\boldsymbol{\omega}|}$$

to check *a posteriori* that we have separated the total flow into coherent vortex tubes which tend to maximize the relative helicity due to vortex stretching and incoherent background flow which tends to maximize dissipation on vortex sheets where helicity is zero (Figure 10b, left). These observations are consistent with Moffatt's conjecture stating that: '*Blobs of maximal helicity may be interpreted as coherent structures, separated by regular surfaces on which vortex sheets, the site of strong dissipation, may be located*' [35].

We have shown that the coherent flow contains the vortex tubes and has the same $k^{-5/3}$ power-law behavior as the total flow. This lead us to propose a new scenario to explain the turbulent cascade. The transfer of energy between the various scales does not result from vortex fragmentation, as in the classical Richardson's scenario. It is rather due to nonlinear vortex interactions, e.g., stretching and straining, which transfer coherent energy throughout the whole inertial range, while at the same time producing incoherent energy which is dissipated at the smallest scales. We have obtained similar results for other homogeneous isotropic three-dimensional turbulent flows [17, 18] and for three-dimensional turbulent mixing layers [44], which are consistent with our interpretation of the turbulent cascade.

5. Conclusion

For more than ten years we have been developing a research program based on the wavelet representation to analyse, compute and model fully-developed turbulent flows. This has lead us to propose a new method, called Coherent Vortex Simulation, to compute their time evolution. CVS is in the spirit of Ha Minh's semi-deterministic model because it splits the flow into coherent and incoherent components, with the difference that CVS filtering is nonlinear and thus depends on each flow realization.

The coherent vortex extraction is done by nonlinearly filtering the wavelet coefficients of the vorticity, which is chosen since it is better suited than velocity for dynamical, topological and invariance reasons. The multiscale property of the wavelet representation is essential to extract all the active scales of coherent vortices, in particular their small scales which are excited during nonlinear vortex

interactions. Classical methods, such as LES, only extract the larger scales of the coherent vortices and thus eliminate their small scales. As a result, subgrid scale models have difficulties to model them correctly, since the small scales attached to the coherent vortices may be nonlinearly active and thus cause backscatter. The CVS filter avoids this problem, since it controls that the discarded modes, corresponding to the incoherent random background, are structureless and have reached a statistical equilibrium characterized by a Gaussian PDF for vorticity in 2D (and for velocity in 3D), together with an enstrophy equipartition in 2D (and an energy equipartition in 3D). Indeed, the stirring of the incoherent background flow by the coherent vortices guarantees its statistical stationarity, homogeneity and ergodicity. Moreover, we have shown that for two-dimensional turbulent flows the nonlinear instabilities are inhibited in the background flow by the strain the coherent vortices exert on it, and thus the incoherent background flow is slaved to the coherent vortices. We have conjectured that this is also true for three-dimensional turbulent flows. In contrast to the incoherent modes, the coherent vortices are not in statistical equilibrium, and therefore their evolution cannot be statistically modelled, but is deterministically computed in a wavelet basis which dynamically adapts to the regions where strong gradients are produced by the nonliner vortex interections.

We have also proposed a new way of forcing turbulent flows, where the injection of both energy and enstrophy is done in wavelet space, i.e., locally in both space and scale. This method seems more sound physically than the classical forcing in Fourier space, since it models the local production of coherent vortices by nonlinear instabilities, such as Kelvin–Helmholtz instability. This wavelet forcing is also used to model the effect of the incoherent background flow on the coherent vortices. To take into account obstacles or complex geometries using CVS, we have chosen the penalization method, which treats them as porous media. As example, we have computed a two-dimensional flow past an array of cylinders for three angles of incidence.

The CVS method can be summarized as follows:

- extraction of coherent vortices, whatever their excited scales;
- computation of their time evolution in an adaptive wavelet basis which dynamically resolves the regions of strong gradients;
- elimination at each time step of the incoherent components produced by the vortex interactions, which models the turbulent dissipation;
- modelling of the effect of the incoherent background flow on the coherent vortices by applying a forcing in wavelet coefficients space.

Applications of CVS to both two and three-dimensional turbulent flows have shown that coherent vortices are well extracted and that the compression thus obtained is important. Moreover, the remaining incoherent background flow exhibits quasi-Gaussian statistics and decorrelation, which guarantees that its effect on the coherent vortices can be statistically modelled. We have applied CVS to

compute a time developing two-dimensional mixing layer and a wavelet forced two-dimensional homogeneous and isotropic turbulent flow. For the former we have compared the CVS results with a pseudo-spectral DNS integrated during 30 initial eddy-turnover times. We found excellent agreement between the solutions obtained with both methods, although the CVS uses 30 times less degrees of freedom than the DNS computed at resolution $N = 256^2$. In particular, all active scales of motions are well resolved, the energy spectra have the same scaling, and the vortex pairings are well predicted in space and time.

In conclusion, CVS is a new semi-deterministic method, intermediate between LES and DNS, which offers the advantage that the number of degrees of freedom is dynamically adapted during the flow evolution and depends on the number of coherent vortices excited by the nonlinear dynamics. This gives hope to significantly reduce the number of degrees of freedom needed to compute high Reynolds turbulent flows. In this paper the CVS method has been demonstrated for two-dimensional turbulent flows at moderate Reynolds number. We plan for future work to implement it for simulating three-dimensional turbulent flows. Moreover, as the number of coherent vortices seems to increase more slowly, for increasing Reynolds number, than the number of degrees of freedom predicted by the statistical theory of homogeneous isotropic turbulence, we expect that the compression obtained with CVS will become more efficient for large Reynolds numbers.

Acknowledgements

We are very grateful to Maurice Meneguzzi for providing us the three-dimensional DNS data, to Giulio Pellegrino and Alexandre Azzalini for performing the coherent vortex extractions, and to Nicholas Kevlahan for fruitful discussions. We thank Joel Ferziger and Alain Bossavit for reading and improving this paper. We acknowledge support from the French-German program Procope (contract 01220ZE), the European TMR program (contract FMRX-CT98-0184) and the program PPF of ENS Paris (contract CR15407).

References

1. Angot, P., Bruneau, C.H. and Fabrie, P., A penalization method to take into account obstacles in viscous flows. *Numer. Math.* **81** (1999) 497–500.
2. Arquis, E. and Caltagirone, J.P., Sur les conditions hydrodynamique au voisinage d'une interface millieux fluide–millieu poreux: Application à la convection naturelle. *C.R. Acad. Sci. Paris II* **299** (1984) 1–4.
3. Burke Hubbard B., *The World According to Wavelets: The Story of a Mathematical Technique in the Making*. AK Peters, Natick, MA (1998).
4. Casella, G. and Berger, R.L., *Statistical Inference*. Wadsworth and Brooks/Cole, Pacific Grove (1990).
5. Daubechies I., *Ten Lectures on Wavelets*. SIAM, Philadelphia, PA (1992).
6. Domaradzki, J.A., Nonlocal triad interactions and the dissipation range of isotropic turbulence. *Phys. Fluids A* **4** (1992) 2037.

7. Donoho, D., Unconditional bases are optimal bases for data compression and statistical estimation. *Appl. Comput. Harmon. Anal.* **1** (1993) 100.
8. Donoho, D. and Johnstone, I., Ideal spatial adaption via wavelet shrinkage, *Biometrica* **81** (1994) 425–455.
9. Farge, M. and Rabreau, G., Transformée en ondelettes pour détecter et analyser les structures cohérentes dans les écoulements turbulents bidimensionnels. *C.R. Acad. Sci. Paris, Série II* **307** (1988) 433.
10. Farge, M., Holschneider, M. and Colonna, J.F., Wavelet analysis of coherent structures in two-dimensional turbulent flows. In: Moffatt, H.K. and Tsinober, A. (eds), *Topological Fluid Mechanics*. Cambridge University Press, Cambridge (1989) pp. 765–776.
11. Farge, M., Wavelet transforms and their applications to turbulence. *Ann. Rev. Fluid Mech.* **24** (1992) 395–457.
12. Farge, M., Goirand, E., Meyer, Y., Pascal, F. and Wickerhauser, M.V., Improved predictability of two-dimensional turbulent flows using wavelet packet compression. *Fluid Dynam. Res.* **10** (1992) 229.
13. Farge, M. and Philipovitch, T., Coherent structure analysis and extraction using wavelets. In: Meyer, Y., Murenzi, R. and Roques, S. (eds) *Progress in Wavelet Analysis and Applications*. Editions Frontières, Paris (1993) p. 477.
14. Farge, M., Kevlahan, N.K., Perrier, V. and Goirand, E., Wavelets and turbulence. *Proc. IEEE* **84**(4) (1996) 639–669.
15. Farge, M., Kevlahan, N.K., Perrier, V. and Schneider, K., Turbulence analysis, modelling and computing using wavelets. In: van den Berg, J.C. (ed.), *Wavelets in Physics* Cambridge University Press, Cambridge (1999) pp. 117–200.
16. Farge, M., Schneider, K. and Kevlahan, N.K., Non-Gaussianity and Coherent Vortex Simulation for two-dimensional turbulence using an adaptive orthonormal wavelet basis. *Phys. Fluids* **11**(8) (1999) 2187–2201.
17. Farge, M., Schneider, K., Pellegrino, G., Wray, A.A. and Rogallo, R.S., CVS decomposition of 3D homogeneous turbulence using orthogonal wavelets. Center for Turbulence Research: Summer Program (2000) pp. 305–317.
18. Farge, M., Pellegrino, G. and Schneider, K., Coherent vortex extraction in 3D turbulent flows using orthogonal wavelets. *Phys. Rev. Lett.* **87**(5) (2001).
19. Ferziger, J.H., Large Eddy Simulation. In: Gatski, T.B., Hussaini, M.Y. and Lumley, J.L. (eds), *Simulation and Modeling of Turbulent Flows*, ICASE Series in Computational Science and Engineering. Springer-Verlag, New York (1992) p. 109.
20. Forestier, M., Etude par méthode spectrale de sillages tridimensionnels en fluide stratifié. Thèse de doctorat, Université de Nice-Sophia Antipolis (2000).
21. Fröhlich, J. and Schneider, K., An adaptive wavelet-vaguelette algorithm for the solution of PDEs. *J. Comput. Phys.* **130** (1997) 174–190.
22. Germano, M., Piomelli, U., Moin, P. and Cabot, W.H., A dynamic subgrid scale model eddy viscosity model. Center for Turbulence Research: Summer Report (1990) pp. 5–17.
23. Glowinski, R., Pan, T.W. and Periaux, J., A fictitious domain method for external incompressible viscous flow modeled by Navier–Stokes equations. *Comput. Methods Appl. Mech. Engrg.* **112** (1994) 3–17.
24. Grossmann, A. and Morlet, J., Decomposition of Hardy functions into square integrable wavelets of constant shape. *SIAM J. Math. Anal.* **15** (1984) 723.
25. Ha Minh H., La modélisation statistique de la turbulence: ses capacités et ses limitations. *C.R. Acad. Sci. Paris, Série IIb* **327** (1999) 343–358.
26. Ha Minh, H. and Kourta, A., Semi-deterministic turbulence modelling for flows dominated by strong organized structures. In: *Proceedings 9th Symposium on Turbulent Shear Flows*, Kyoto, August 16–18 (1993) pp. 10.5.1–10.5.6.

27. Ha Minh, H., Order and disorder in turbulent flows: their impact on turbulence modelling. In: *Osborne Reynolds Centenary Symposium*. UMIST, Manchester (1994) pp. 1–30.
28. Kevlahan, N.K. and Farge, M., Vorticity filaments in two-dimensional turbulence: Creation, stability and effect. *J. Fluid Mech.* **346** (1997) 49–76.
29. Kevlahan, N.K. and Ghidaglia, J.M., Computation of turbulent flow past an array of cylinders using a spectral method with Brinkman penalization. *Eur. J. Mech. B/Fluids* **20** (2001) 333–350.
30. Kraichnan, R.H., Inertial ranges of two-dimensional turbulence. *Phys. Fluids* **10** (1967) 1417–673.
31. Leonard, A., Energy cascade in Large Eddy Simulations of turbulent fluid flows. *Adv. Geophys.* **18A** (1974) 237.
32. Lemarié, P.G. and Meyer, Y., Ondelettes et bases Hilbertiennes, *Rev. Math. Ibero Am.* **2** (1986) 1.
33. Mallat, S., *A Wavelet Tour of Signal Processing*. Academic Press, New York (1998).
34. Méneveau, C., Analysis of turbulence in the orthonormal wavelet representation. *J. Fluid Mech.* **232** (1991), 469.
35. Moffatt, H.K., Magnetostatic equilibria and analogous Euler flows of arbitrarily complex topology. *J. Fluid Mech.* **150** (1985), 359.
36. Peskin, C.S., Numerical analysis of blood flow around heart valves: A numerical study. *J. Comput. Phys.* **10** (1972) 252.
37. Reynolds, O., On the dynamical theory of incompressible viscous fluids and the determination of the criterion. *Philos. Trans. Roy. Soc. London* **186** (1894) 123.
38. Reynolds, W.C. and Hussain, A.K.M.F., The mechanism of an organized wave in turbulent shear flow. *J. Fluid Mech.* **54** (1971) 263–288.
39. Schneider, K., Kevlahan, N. and Farge, M., Comparison of an adaptive wavelet method and nonlinearly filtered pseudo-spectral methods for two-dimensional turbulence. *Theoret. Comput. Fluid Dynam.* **9** (1997) 191–206.
40. Schneider, K. and Farge, M., Wavelet approach for modelling and computing turbulence. In: *Lecture Series 1998–05: Advances in Turbulence Modelling*, von Karman Institute for Fluid Dynamics, Bruxelles (1998) pp. 1–132.
41. Schneider, K., Farge, M. and Kevlahan, N., Spatial intermittency in two-dimensional turbulence: A wavelet approach. *J. Fluid Mech.* (2001) (submitted).
42. Schneider, K. and Farge, M., Wavelet forcing for numerical simulation of two-dimensional turbulence. *C.R. Acad. Sci. Paris, Série IIb* **325** (1997) 263–270.
43. Schneider, K. and Farge, M., Numerical simulation of a temporally growing mixing layer in an adaptive wavelet basis. *C.R. Acad. Sci. Paris, Série II b* **328** (2000) 263–269.
44. Schneider, K., Farge, M., Pellegrino, G. and Rogers, M., CVS filtering of 3D turbulent mixing layers using orthogonal wavelets. Center for Turbulence Research: Summer Program (2000) pp. 319–330.
45. Schneider, K., Modélisation et simulation numérique en base d'ondelettes adaptatives, applications en mécanique des fluides et en combustion. Habilitation à diriger des recherches, Université Louis Pasteur, Strasbourg (2001) pp. 16–19.
46. Schneider, K. and Farge, M., Coherent Vortex Simulation (CVS) of two-dimensional flows in complex geometries. Preprint CMI, Université de Provence, Marseille (2001).
47. Vincent, A. and Meneguzzi, M., The spatial structure and statistical properties of homogeneous turbulence. *J. Fluid Mech.* **225** (1991) 1–20.
48. Winckelmans, G.S., Some progress in large-eddy simulation using the 3D vortex particle method. Center for Turbulence Research: Annual Research Briefs (1995) pp. 391–415.